ISSN 1063-7745, Crystallography Reports, 2012, Vol. 57, No. 7, pp. 943–947. © Pleiades Publishing, Inc., 2012.

NANOMATERIALS

Phase Trajectories in $CaO–Al_2O_3–SiO_2$ Melts

V. I. Lutsyk, A. E. Zelenaya, and V. V. Savinov

Institute of Physical Materials Science, Siberian Branch, Russian Academy of Sciences, Sakhyanova ul. 6, Ulan-Ude, 670047

e-mail: vluts@pres.bscnet.ru

Received December 20, 2010

Abstract—A technique for constructing a phase diagram of the $CaO–Al_2O_3–SiO_2$ system on a computer using the kinematic approach to describe surfaces is proposed. The geometric structure of the diagram and its phase regions is described. Crystallization paths are considered for different parts of the diagram.

DOI: 10.1134/S1063774512070176

INTRODUCTION

The $CaO–Al_2O_3–SiO_2$ system is of great practical importance. The development of a computer model of the system will make it possible to not only reproduce the well-studied liquidus surfaces [1–5], but also completely reconstruct its phase diagram, including the ruled surfaces, horizontal planes at temperatures of invariant points, and vertical triangulation planes. This complete model of the system is the basis for obtaining information about the products of interaction between initial components; it allows one to analyze the crystallization stages in all parts of the diagram and consider all phase regions, including solid-phase regions, which are of practical importance for studying ceramic processes.

The existing models of the $CaO–Al_2O_3–SiO_2$ system are aimed at solving certain applied problems; they often disregard its complete topological structure and neglect or distort some surfaces in the diagram [6–8]. The surfaces in the diagram can be approximated using both different thermodynamic approaches [6–10] and mathematical methods, among which we can select polynomial models [11–13], minimum-area surfaces [14], etc.

We chose the kinematic method for describing surfaces in the diagram, which makes it possible to take into account the structure of surfaces of any complexity [15, 16]. A kinematic surface is considered as a set of successive positions of a generatrix that moves in space according to a certain law. The law of motion of the generatrix is determined by the set of directrices.

STRUCTURE OF PHASE DIAGRAM OF $CAO–AL_2O_3–SIO_2$

When developing the model, the initial data were taken as the coordinates of 14 binary points (nine eutectics (e) and five peritectics (p)); 16 ternary points (six eutectics (E), nine quasi-peritectics (Q), and a point of four-phase mass regrouping with the participation of two polymorphs (U)); seven inflection points on univariant liquidus lines ((E_2, E_3), (E_3, E_4), (E_4, E_5), (E_6, E_3), (Q_4, Q_9), (Q_5, Q_6), (Q_7, Q_8)); and ten binary (R_1–R_{10}) and two ternary (R_{11} and R_{12}) compounds (Fig. 1). The compounds are denoted as follows: (R_1) $3CaO \cdot SiO_2$, (R_2) $2CaO \cdot SiO_2$, (R_3) $3CaO \cdot 2SiO_2$, (R_4) $CaO \cdot SiO_2$, (R_5) $3Al_2O_3 \cdot 2SiO_2$, (R_6) $3CaO \cdot Al_2O_3$, (R_7) $5CaO \cdot 3Al_2O_3$, (R_8) $CaO \cdot Al_2O_3$, (R_9) $CaO \cdot 2Al_2O_3$, (R_{10}) $CaO \cdot 6Al_2O_3$, (R_{11}) $2CaO \cdot Al_2O_3 \cdot SiO_2$, ($R_{12}$) $CaO \cdot Al_2O_3 \cdot 2SiO_2$. R_1, R_3, R_6, and R_{10} are incongruently melting compounds and R_2, R_4, R_5, R_7, R_8, R_9, R_{11}, and R_{12} are congruently melting compounds.

The phase diagram is formed by the immiscibility dome (i: k^0nkm) and 16 liquidus surfaces, incluidng S_1: $CaOp_1Q_1p_4$, S_2: $p_4Q_1Q_2Q_3e_6$, S_3: $E_6Q_3E_1e_7R_7$, S_4: $e_7E_1Q_4Q_5e_8R_8$, S_5: $e_8Q_5(Q_5, Q_6)Q_6e_9$, S_6: $e_9Q_6E_6Q_7p_5$, S_7: $Al_2O_3p_5Q_7(Q_7, Q_8)Q_8e_5$, S_8: $p_1Q_1Q_2e_1$, S_9: $e_1Q_2Q_3E_1Q_4(Q_4, Q_9)Q_9p_2R_2$, S_{10}: $p_2Q_9E_2e_2$, S_{11}: $e_2E_2(E_2, E_3)E_3(E_3, E_4)E_4e_3R_4$, S_{12}: $Q_4Q_5(Q_5, Q_6)Q_6E_6E_3(E_2, E_3)E_2Q_9$, S_{13}: $E_3(E_3, E_4)E_4(E_4, E_5)E_5Q_8(Q_7, Q_8)Q_7E_6$, S_{14}: $e_3E_4(E_4, E_5)E_5Up_3$, S_{15}: $SiO_2mknp_3Ue_4$, and S_{16}: $e_4UE_5Q_8e_5R_5$ (Fig. 1a). The phase diagram is formed by the immiscibility dome (i: k^0nkm) and 16 liquidus surfaces (Fig. 1a), including 80 ruled surfaces (Fig. 1b); 16 horizontal planes at temperatures of invariant points (H) (Fig. 1c); and 16 triangulation vertical planes (V), which divide the diagram into 15 subsolidus regions (Fig. 1d).

PHASE REGIONS

Sixteen invariant transformations occur in the system under study, including nine quasi-peritectic transformations, six eutectic transformations, and one transformation with regrouping of two polymorphic modifications: $L(Q_8) + Al_2O_3 \rightarrow R_5 + R_{12}$, $L(Q_5) + R_9 \rightarrow R_8 + R_{11}$, $L(Q_7) + Al_2O_3 \rightarrow R_{10} + R_{12}$, $L(Q_6) + R_9 \rightarrow R_{10} + R_{11}$, $L(Q_1) + CaO \rightarrow R_1 + R_6$, $U + SiO_2^{cr} \rightarrow R_5 + SiO_2^{tr}$, $L(Q_2) + R_1 \rightarrow R_2 + R_6$, $L(E_6) \rightarrow R_{10} +$

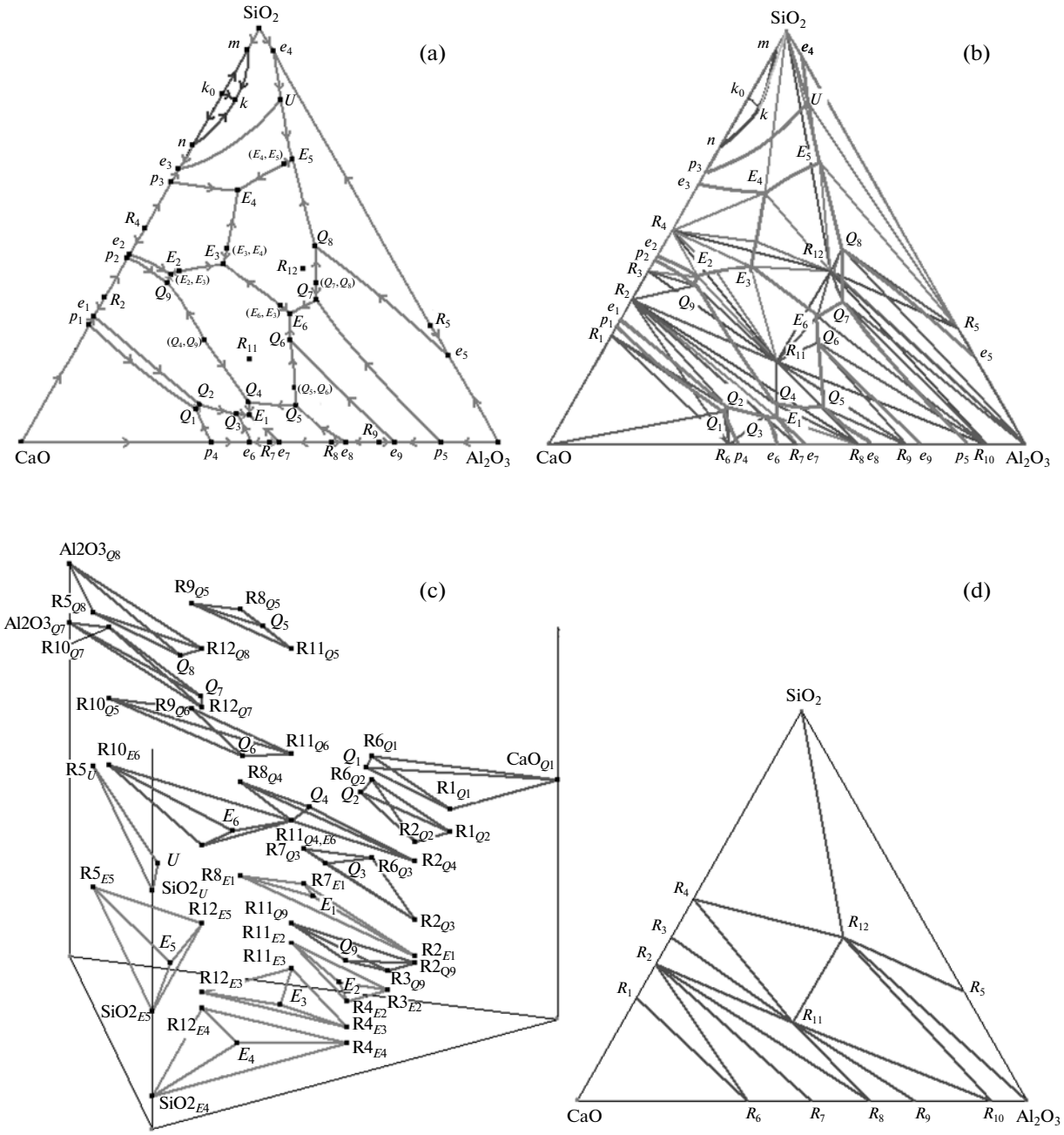

Fig. 1. *XY* projections of (a) liquidus surfaces and immiscibility dome and (b) all surfaces of the diagram, (c) spatial scheme of arrangement of horizontal planes, and (d) partition into subsolidus regions.

$R_{11} + R_{12}$, $L(Q_4) + R_{11} \rightarrow R_2 + R_8$, $L(Q_3) + R_6 \rightarrow R_2 + R_7$, $L(E_5) \rightarrow R_5 + R_{12} + SiO_2$, $L(E_1) \rightarrow R_2 + R_7 + R_8$, $L(Q_9) + R_2 \rightarrow R_3 + R_{11}$, $L(E_2) \rightarrow R_3 + R_4 + R_{11}$, $L(E_3) \rightarrow R_4 + R_{11} + R_{12}$, $L(E_4) \rightarrow R_4 + R_{12} + SiO_2$.

The phase diagram under consideration contains one single-phase region L; 33 two-phase regions: $L_1 + L_2$, $L + CaO$, $L + R_1$, $L + R_2$, $L + R_3$, $L + R_4$, $L + R_5$, $L + R_6$, $L + R_7$, $L + R_8$, $L + R_9$, $L + R_{10}$, $L + R_{11}$, $L + R_{12}$, $L + SiO_2^{cr}$, $L + SiO_2^{tr}$, $L + Al_2O_3$, $R_1 + R_6$, $R_2 + R_6$, $R_2 + R_7$, $R_2 + R_8$, $R_2 + R_{11}$, $R_3 + R_{11}$, $R_4 + R_{11}$, $R_5 + R_{12}$, $R_8 + R_{11}$, $R_9 + R_{11}$, $R_{10} + R_{11}$, $R_{10} + R_{12}$, $R_{11} + R_{12}$, $R_4 + R_{12}$, $R_{12} + SiO_2$, and $R_{12} + Al_2O_3$; and 46 three-phase regions: $L_1 + L_2 + SiO_2$, $L + CaO + R_1$, $L + CaO + R_6$, $L + R_1 + R_2$, $L + R_1 + R_6$, $L + R_2 + R_3$, $L + R_2 + R_6$, $L + R_2 + R_7$, $L + R_2 + R_8$, $L + R_2 + R_{11}$, $L + R_3 + R_4$, $L + R_3 + R_{11}$, $L + R_4 + R_{11}$, $L + R_4 + R_{12}$, $L + R_4 + SiO_2^{cr}$, $L + R_5 + R_{12}$, $L + R_5 + SiO_2^{u}$, $L + R_5 + SiO_2^{d}$, $L + R_5 + Al_2O_3$, $L + R_6 + R_7$, $L + R_7 + R_8$, $L + R_8 + R_9$, $L + R_8 + R_{11}$, $L + R_9 + R_{10}$, $L + R_9 + R_{11}$, $L + R_{10} + R_{11}$, $L + R_{10} + R_{12}$, $L + R_{11} + R_{12}$, $L + R_{10} + Al_2O_3$, $L + R_{12} + Al_2O_3$, $L + R_{12} + SiO_2$, $CaO + R_1 + R_6$, $R_1 + R_2 + R_6$, $R_2 + R_3 + R_{11}$, $R_2 + R_6 + R_7$, $R_2 + R_7 + R_8$,

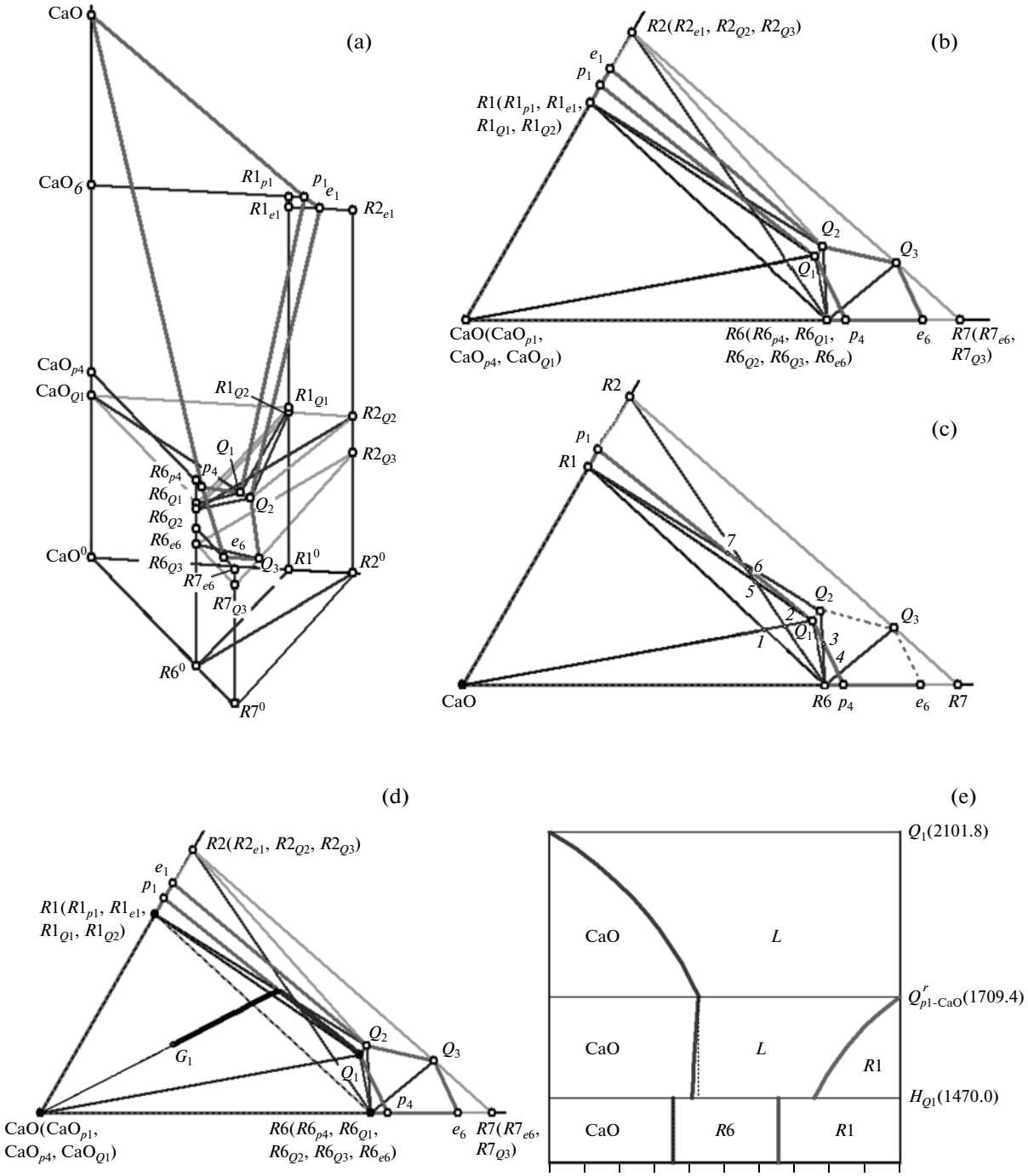

Fig. 2. (a) Spatial fragment of the diagram; (b) *XY* projection; (c) partition into concentration fields; and (d–i) crystallization paths and material-balance diagrams for the (d, e) G_1, (f, g) G_2, and (h, i) G_3 melts.

$R_2 + R_8 + R_{11}$, $R_3 + R_4 + R_{11}$, $R_4 + R_{11} + R_{12}$, $R_4 + R_{12} + SiO_2$, $R_5 + R_{12} + SiO_2$, $R_5 + R_{12} + Al_2O_3$, $R_8 + R_9 + R_{11}$, $R_9 + R_{10} + R_{11}$, $R_{10} + R_{11} + R_{12}$, and $R_{10} + R_{12} + Al_2O_3$.

CONCENTRATION FIELDS AND CRYSTALLIZATION PATHS

When projecting all elements of the diagram, the composition of the triangle is divided into concentration fields that differ in the stages of crystallization [17]. For the $CaO–Al_2O_3–SiO_2$ system under consideration, 117 two-dimensional, 163 one-dimensional, and 45 point fields were selected (Fig. 1b). In view of the complex structure of the $CaO–Al_2O_3–SiO_2$ system, a limited number of crystallization paths are generally analyzed [4], whereas the model proposed makes it possible to consider phase trajectories for all concentration fields of the diagram.

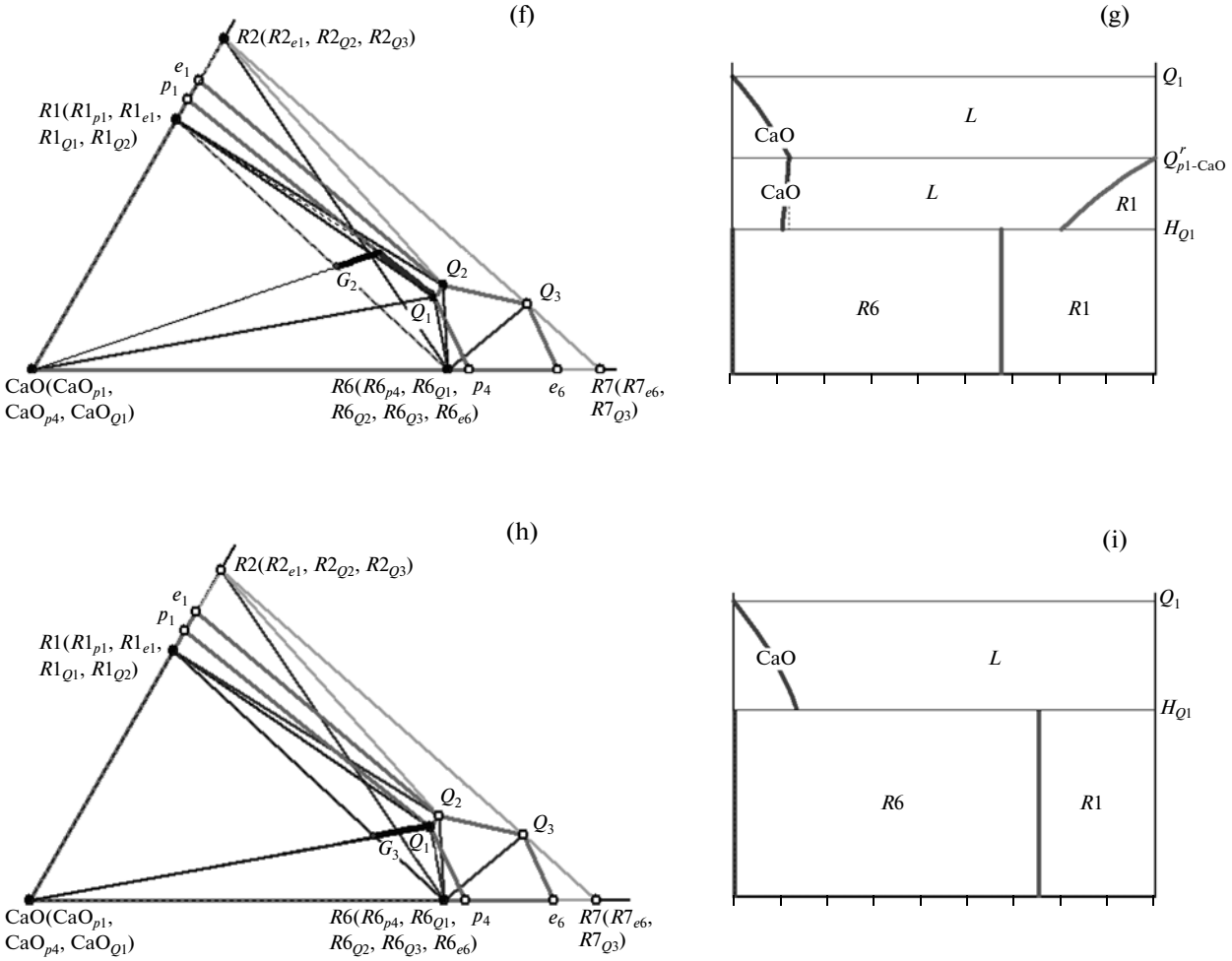

Fig. 2. (Contd.)

Let us consider the trajectories of the melts that are specified in the crystallization field of the CaO component (Figs. 2a, 2b) but fall in the concentration fields of different dimensions. Being projected, the chosen liquidus surface $S_1(\mathrm{CaO}p_1Q_1p_4)$ is divided by the elements of the diagram into 12 two-dimensional, 20 one-dimensional, and 7 one-dimensional fields (Fig. 2c).

When passing through the two-phase region L + CaO, the melt $G_1(0.8; 0.1; 0.1)$ within the triangle $R_1R_6\mathrm{CaO}$ (in the two-dimensional field CaO-$R1$-1) (Fig. 2d) moves along the straight line CaO-G_1 (on the concentration projection) to the liquidus line p_1Q_1. Then, it enters the region L + CaO + $R1$ and moves along the univariant equilibrium line p_1Q_1. The reaction $L(Q_1) + \mathrm{CaO} \rightarrow R_1 + R_6$ ends with a deficit of melt on the horizontal complex $R_1Q_1R_6\mathrm{CaO}$ at a temperature of Q_1, below which CaO, R_1, and R_6 crystals remain. The crystallization stages can additionally be considered using material-balance diagrams (Fig. 2e). In particular, the G_1 composition under study intersects the liquidus surface S_1 at 2101.8° and enters the region L + CaO, where the fraction of the L phase decreases, while the fraction of CaO increases. At 1709.4°, the point G_1 reaches the ruled surface $S^r_{p1\text{-CaO}}$ and enters the region L + CaO + $R1$, where the fraction of the R_1 phase increases, while the fraction of L and CaO decreases. When the point G_1 reaches the horizontal plane at a temperature of Q_1 (1470°), the L phase disappears and, below this temperature, the composition enters the region CaO + R_1 + R_6.

The crystallization paths for the composition $G_2(0.67; 0.11; 0.22)$, which is located on the $R1R6$ line (in the one-dimensional field $R1$-1), are similar (Fig. 2f). However, below the horizontal complex $R_1Q_1R_6\mathrm{CaO}$, the composition falls in the two-phase region $R1$ + $R6$ (Fig. 2h).

The composition $G_3(0.65; 0.07; 0.28)$ is set at the intersection of the projection of the tie-line $\mathrm{CaO}Q_1$ and the $R1R6$ line at point 1 (in the point field) (Fig. 2h). The G_3Q_1 line corresponds to the transmission of melt through the two-phase region L + CaO.

Then, the composition arrives directly at the two-phase region $R1 + R6$ (Fig. 2i).

For the compositions that are also located near the liquidus surface S_1 but within the triangle $R1R2R6$ (i.e., in the fields $R1$-1-2-5, $R1$-5-6-7, $R1$-7-p_1, or $R6$-1-2) (Fig. 2b) the crystallization paths come to end at the temperature of the point Q_2. The reaction $L(Q_2) + R_1 \rightarrow R_2 + R_6$ ends in the $R_1R_2Q_2R_6$ plane with a deficit of melt, and only the R_1, R_2, and R_6 crystals remain below. If the compositions fall in the triangle $R2R6R7$ (i.e., in the fields Q_1-2-5, Q_1-5-6, $R6$-Q_1-2, $R6$-Q_1-3, $R6$-3-4, or $R6$-4-p_4), the melt trajectories reach the point Q_3. The reaction $L(Q_3) + R_6 \rightarrow R_2 + R_7$ ends at the complex $R_6R_2Q_3R_7$, and the R_2, R_6, and R crystals remain below.

Similarly, any other parts of the diagram can be considered and crystallization paths for an arbitrary composition can be obtained.

CONCLUSIONS

Conventional textbooks on materials science consider no more than ten versions of crystallization paths for the system under consideration [4].

The computer model presented here makes it possible to consider crystallization paths for all concentration fields of the diagram, which include 117 two-dimensional, 163 one-dimensional, and 45 point fields. Material balance diagrams allow one to trace additionally the crystallization stages and estimate the phase fractions.

Note that the proposed model of the phase diagram of $CaO–Al_2O_3–SiO_2$ system not only expands the possibilities of its study but can also serve as a basis for constructing silicate systems of a similar topological type ($MgO–Al_2O_3–SiO_2$, $Y_2O_3–Al_2O_3–SiO_2$, $FeO–Al_2O_3–SiO_2$).

REFERENCES

1. A. L. Gentil and W. R. Foster, J. Am. Ceram. Soc. **46**, 14 (1963).
2. E. M. Levin, C. R. Robbins, and H. F. McMurdie, *Phase Diagrams for Ceramists* (American Ceramic Society, Ohio, 1964).
3. N. A. Toropov, V. P. Barzakovskii, V. V. Lapshin, et al., *Phase Diagrams of Silicate Systems: A Handbook,* Issue 3: *Ternary Silicate Systems* (Nauka, Leningrad, 1972) [in Russian].
4. *Physical Chemistry of Silicates,* Ed. by A. A. Pashchenko (Vishcha shkola, Kiev, 1977) [in Russian].
5. K. A. Subbotin, E. V. Zharikov, L. D. Iskhakova, and S. V. Lavrishchev, Crystallogr. Rep. **46**, 1030 (2001).
6. V. Danek, *Physico-Chemical Analysis of Molten Electrolytes* (Elsevier, 2006).
7. R. G. Berman and T. H. Brown, Geochim. Cosmochim. Acta **48**, 661 (1984).
8. K. Shobu, CA*L*PHAD **33**, 279 (2009).
9. B. Cheynet, C. Bonnet, and M. Stankov, CA*L*PHAD **33**, 312 (2009).
10. G. F. Voronin, Zh. Fiz. Khim. **79**, 2126 (2005).
11. H. Scheffe, J. R. Statistical Soc. **20**, 344 (1957).
12. *Application of Mathematical Methods for Studying Multicomponent Systems,* Ed. by G. Zedginidze (Metallurgiya, Moscow, 1974) [in Russian].
13. A. A. Vecher, Dokl. Akad. Nauk BSSR **27**, 59 (1983).
14. A. A. Tuzhilin and A. T. Fomenko, *Elements of Geometry and Topology of Minimum Surfaces* (Nauka, Moscow, 1991) [in Russian].
15. V. I. Lutsyk, A. E. Zelenaya, and A. M. Zyryanov, Crystallogr. Rep. **54**, 1300 (2009).
16. V. I. Lutsyk, A. M. Zyryanov, and A. E. Zelenaya, Zh. Neorg. Khim. **53**, 858 (2008).
17. V. I. Lutsyk and V. P. Vorob'eva, Zh. Neorg. Khim. **40**, 1697 (1995).

Translated by Yu. Sin'kov